

1 Submitted to Journal of the American Oil Chemists' Society, 2022.

2

3

4

5 **“Selective synthesis of a valuable unsaturated fatty alcohol via catalytic**
6 **and non-catalytic liquid-phase methyl oleate reduction”**

7

8

9

By

10

11 *Alejandro Vallejo Orrego^a, Cristián A. Ferretti^b and Verónica K. Díez^{a*}*

12

13

14

15 ^a Catalysis Science and Engineering Research Group (GICIC), Research Institute of
16 Catalysis and Petrochemistry (INCAPE), UNL-CONICET, CCT CONICET Santa Fe,
17 Colectora Ruta Nac. 168, km 0, Paraje "El Pozo", (3000) Santa Fe, Argentina

18

19 ^b Fester Laboratory of Organic Chemistry, Institute of Applied Chemistry of Litoral,
20 IQAL, UNL-CONICET, Santiago del Estero 2829, (3000) Santa Fe, Argentina

21

22

23 *Corresponding author. Tel.: +54 342 4511546, Ex 6118; Fax: +54 342 4511170.

24 E-mail address: verodiez@fiq.unl.edu.ar (V.K. Díez).

25 **Abstract**

26 The upgrading of oleyl alcohol synthesis via methyl oleate reduction using NaBH₄
27 without H₂ supply was investigated. It was possible to synthesize selectively the valuable
28 unsaturated fatty alcohol with high yields. Non-catalytic and catalytic experiments were
29 developed trying to improve the low final oleyl alcohol yield previously obtained. The
30 effect of reaction temperature, methyl oleate/NaBH₄ molar ratio and properties of
31 different catalysts on final oleyl alcohol yield was analyzed. Thus, alumina-supported
32 metal (M) catalysts (M = Fe, Ce, Mo) were synthesized by impregnation at incipient
33 wetness. The M/Al₂O₃ catalysts were characterized in their chemical, textural, structural
34 and acid-base properties using ICP, N₂ physisorption, XRD and NH₃ and CO₂ TPD.
35 During non-catalytic methyl oleate reduction final methyl oleate conversion and oleyl
36 alcohol yield of 94% were obtained using a methyl oleate/NaBH₄ molar ratio of 0.11 at
37 333 K. Catalytic activity of M/Al₂O₃ solids did not correlate with basic site number but
38 increased as acid site number and ionic potential of M cations increase. This suggests that
39 cations with high acid site number and polarizing power are the ones that promote the
40 polarization of the ester C=O and anion [BH₄]⁻ bonds favoring de methyl oleate
41 conversion. In addition, the reaction mechanism for fatty acid methyl ester reduction was
42 investigated from a theoretical approach using Density Functional Theory method at
43 B3LYP/6-31++G(d,p) computational level. Results obtained during theoretical
44 calculations confirmed that the formation of reducing alkoxyborohydride species is
45 energetically favored and allowed to understand the events at microscopic level involved
46 in the reaction mechanism.

47

48 **Keywords: methyl oleate; oleyl alcohol; sodium borohydride; reduction reaction**
49 **mechanism; DFT calculations**

50 **1. Introduction**

51 Natural fatty alcohols (FOL) are linear, monohydric, saturated or unsaturated carbon
52 compounds and have carbon chains between C6-C22. These fatty alcohols are obtained
53 from renewable sources such as animal or vegetable fats, waxes and oils. Fatty alcohols,
54 due to their amphiphilic character (combination of nonpolar carbon chain with polar
55 hydroxyl group), exhibit surface and interface activity, which allows their use in
56 emulsions and microemulsions [Noweck, 2011], favoring their use in personal care and
57 cosmetic industries taking part in the formulation of liquid soaps, shampoos, conditioners,
58 skin emollients, emulsifiers and densifiers of creams and lotions. Thus, fatty alcohols are
59 employed in ionic and non-ionic surfactant production [Sad et al., 2007]. In particular,
60 fatty alcohol sulfates and fatty alcohol ether sulfates belong to the group of anionic
61 surfactants. In addition, fatty alcohol polyglycoethers and fatty alcohol ethoxilates are
62 the first non-ionic surfactants manufactured in technical scale, being the ethoxilates
63 compounds better low-foaming surfactants than the former. Alkyl polyglucosides are
64 manufactured from fatty alcohols and sugar molecules following various procedures.
65 These FOL-derived surfactants are surface active agents which have wide industrial
66 applications as cleaning agents and detergents.

67 Industrially, natural FOL are synthesized by conversion of fatty acid methyl esters
68 (FAME) and fatty acids (FA) via catalytic hydrogenation reaction. In these processes
69 severe reaction conditions are used that involve high temperatures (473-573 K), high
70 pressures of H₂ (20-30 MPa), and solid catalysts based mainly on chromium, such as Cu-
71 Cr [Miya, 1981] and Zn-Cr [Rieke et al., 1997; Rieke et al., 1997], which resulted
72 selective to FOL but is harmful to the environment due to the pollution generated by the
73 final disposal of Cr. Due that, in recent years research has been directed at studying
74 catalysts with similar catalytic activities, which are more efficient and generate less

75 pollution, mainly using catalysts based on noble metals. In fact, when using Ru-Sn/Al₂O₃
76 bimetallic catalysts, a high FOL selectivity is obtained by hydrogenation of methyl laurate
77 using milder reaction conditions (523 K, 5.6 MPa of H₂) [Toba et al., 1999]. In addition,
78 other authors using a similar Ru-Sn/Al₂O₃ catalyst, obtained stearyl alcohol (saturated
79 alcohol) with final yields up to 96% by hydrogenation of C=C and C=O bonds of methyl
80 oleate under severe reaction conditions (553 K, 10 MPa of H₂) [Tahara et al., 1996]. On
81 the other hand, when hydrogenating fatty acids (decanoic acid) over Re₂O₇, low
82 conversions and moderate selectivities to 1-decanol are achieved using 403 K and 10 MPa
83 of H₂ [Yoshino et al., 1990]. There are excellent results in the synthesis of FOL via
84 hydrogenation of FAME or FA, however, expensive noble metal-based catalysts and high
85 temperatures and H₂ pressures are required.

86 On the other hand, FAME reductions using mild reaction conditions via hydrogen and
87 hydride transfer in the liquid phase and without supplying gaseous H₂ have been studied
88 using homogeneous catalysis and there is practically no information related to the use of
89 heterogeneous catalysis in these reaction processes. In this sense, different authors have
90 demonstrated that metal hydrides are efficient carbonyl compounds reducing agents in
91 presence of alcohols of short carbon chain [Soai et al., 1982; Soai et al., 1984; Brown et
92 al., 1982; Rajeswara Rao et al., 1987; Xu et al., 2010]. Brown et al. [Brown et al., 1982]
93 studied the conversion of ethyl caproate and ethyl benzoate using NaBH₄, LiAlH₄ and
94 Ca(BH₄)₂ and alcohols such as ethanol and 2-propanol. In addition, Soai et al. [Soai et al.,
95 1982; Soai et al., 1984] investigated the esters and lactones reduction employing NaBH₄
96 and different solvent mixtures (tert-butanol/methanol, tetrahydrofuran/methanol).
97 Rajeswara et al. [Rajeswara Rao et al., 1987] and Xu et al. [Xu et al., 2010] investigated
98 the synthesis of FOL from FAME using NaBH₄ or LiAlH₄ and methanol achieving final

99 FOL yields between 35-96%. Thus, high ester conversions and alcohol selectivities have
100 been obtained in all these studies.

101 In addition, in a previous work [Vallejo Orrego et al., 2020] we managed to selectively
102 synthesize different FOL during non-catalytic experiments using mild reaction conditions
103 via hydrogen transfer and hydride without supplying H₂ gas. These results allowed us to
104 determine the role played by the hydride donor (metal hydride) and the hydrogen donors
105 (short carbon chain alcohols) in the fatty acid methyl ester reduction. Particularly, we
106 investigated the effect of fatty acid methyl ester structure using methyl laurate (ML),
107 methyl myristate (MM) and methyl oleate (MO). Experiments were carried out at 323 K
108 employing molar ratios methanol/NaBH₄ and FAME/NaBH₄ of 6.0 and 0.36,
109 respectively, and NaBH₄/Al₂O₃ as reducing solid. Results obtained in that reaction
110 conditions showed that final ML and MM conversions varied between 90.8 and 93.0%
111 while MO final conversion resulted significantly lower (34.5%).

112 Taking into account these previous results, in the present work we report on results
113 obtained during the upgrading of oleyl alcohol synthesis via methyl oleate reduction using
114 NaBH₄ as reducing agent without H₂ supply. Our goal is to continue the research related
115 to the synthesis of oleyl alcohol by carrying out non-catalytic and catalytic experiments
116 trying to improve the low final FOL yield previously obtained. Thus, catalysts based on
117 different M metals (M = Fe, Ce, Mo) supported on γ -Al₂O₃ were synthesized,
118 characterized, and tested in the MO liquid phase reduction reaction. The effect of reaction
119 conditions and the presence of different catalysts on final oleyl alcohol yield were
120 analyzed. In addition, the mechanism of reaction steps involved in non-catalytic reduction
121 of methyl oleate with NaBH₄ was investigated from a theoretical approach using density
122 functional theory (DFT) method at B3LYP/6-31++G(d,p) computational level.

123

124 **2. Materials and experimental procedures**

125 **2.1. Chemicals and solid materials**

126 The commercial fatty acid methyl ester, methyl oleate (Sigma-Aldrich, 99%) was used
127 without further purification. Fatty alcohol, oleyl alcohol (Sigma-Aldrich, $\geq 99\%$) was
128 employed for identification purpose. Methanol (Cicarelli, 99.8%) was used without any
129 purification.

130 The external standard n-hexadecane (Sigma-Aldrich, 99%) and the solvent
131 tetrahydrofuran, THF (Biopack, $\geq 99\%$) were used during tests.

132 Sodium borohydride, NaBH_4 (analytical grade) was purchased from Biopack.

133

134 **2.2. Catalyst synthesis**

135 Alumina-supported metal catalysts ($\text{MO}_x/\text{Al}_2\text{O}_3$, with $\text{M} = \text{Ce}, \text{Fe}, \text{Mo}$), containing
136 around 8.0 wt.% of metal were prepared by incipient wetness impregnation of commercial
137 $\gamma\text{-Al}_2\text{O}_3$ Cyanamid Ketjen CK 300 with aqueous solutions of different metal precursors.
138 Metal precursors used were $\text{Ce}(\text{NO}_3)_3 \cdot 6\text{H}_2\text{O}$ (Fluka, $\geq 99\%$), $\text{Fe}(\text{NO}_3)_3 \cdot 9\text{H}_2\text{O}$ (Anedra,
139 99%) and $\text{Na}_2\text{MoO}_4 \cdot 2\text{H}_2\text{O}$ (Merck, 98%), respectively. The catalyst precursors were
140 thermally treated in flowing air at 673 K during 5 h with the exception of the one
141 containing molybdenum that was treated at 773 K. Catalysts were denoted as $x\text{MAI}$,
142 where x is the metal content expressed in wt.%.

143 The $\gamma\text{-Al}_2\text{O}_3$ pellets were crushed and sieved retaining particles between 180-480 μm .
144 The powdered alumina was thermally treated at 773 K in flowing air for 5 h to remove
145 adsorbed water before the impregnation procedures.

146

147 **2.3. Catalyst characterization**

148 BET surface areas (SA) of catalysts were measured by N₂ physisorption at 77 K using
149 an Autosorb Quantachrome 1-C sorptometer. After calcination, the chemical content of
150 metal was analyzed by inductively coupled plasma (ICP-OES).

151 The structural properties of solid materials were analyzed by X-Ray Diffraction (XRD)
152 technique using a Shimadzu XD-D1 instrument with nickel filtered Cu K α radiations
153 between 10 and 80°.

154 Total acid site number (n_a , $\mu\text{mol/g}$) were determined by TPD of NH₃ preadsorbed at
155 373 K. Samples were thermally treated in Heat the corresponding calcination temperature
156 and then exposed to a 1.11% NH₃/He flow at 373 K during 30 min to enable surface
157 saturation. Weakly adsorbed NH₃ was removed by flushing with He. The temperature
158 was then increased at a rate of 10 K/min from 373 K to 593 K and kept constant for 1 h.
159 NH₃ concentration in the reactor effluent was monitored by a mass spectrometer (MS)
160 detector in a Baltzers Omnistar unit.

161 Total basic site number (n_b , $\mu\text{mol/g}$) were measured by temperature-programmed
162 desorption (TPD) of CO₂ preadsorbed at room temperature. Samples were pretreated in
163 situ in a N₂ flow at 773 K, cooled to room temperature, and then exposed to a flowing
164 mixture of 3% of CO₂/N₂ until surface saturation was achieved (5 min). Weakly adsorbed
165 CO₂ was removed by flushing in N₂. Finally, the temperature was increased to 773 K at
166 a ramp rate of 10 K/min. Desorbed CO₂ was converted in CH₄ on a methanation catalyst
167 (Ni/Kieselghur), then analyzed using a flame ionization detector (FID).

168

169 **2.4. Experimental procedure for methyl oleate reduction**

170 Typical non-catalytic and catalytic reduction reactions of methyl oleate (MO) with
171 methanol and pure NaBH₄ and $x\text{MAI}$ catalyst-supported NaBH₄ were carried out.
172 Reaction temperatures between 308 K and 333 K and atmospheric pressure were used in

173 a semi batch four-necked glass reactor. A solution of MO in tetrahydrofuran (THF)
174 solvent with FAME/THF = 0.017 (molar ratio) was firstly loaded in the reactor. The
175 reactor was permanently exposed to an inert gas stream (flowing N₂). The reaction
176 mixture was warmed up to the reaction temperature. Magnetic stirring (700 rpm) was
177 used. The absence of solubilization problems of MO in the THF solvent under the reaction
178 conditions used was evidenced in the experiments. Thus, a single phase was observed
179 once all the reactants were added to the reactor at the reaction temperatures used.

180 During typical catalytic test an amount of 0.7 g of sodium borohydride (NaBH₄) was
181 added so that the molar ratio FAME/NaBH₄ in the reactor was 0.28. After that, a volume
182 of 5 mL of methanol was added over a period of 1 h reaching a molar ratio
183 alcohol/NaBH₄=6.0. During the 6-hour experiments, 11 samples of ≈ 0.2 mL were
184 extracted from the reactor.

185 Product of reaction was identified using a Thermo Scientific Trace 1300 GC with a
186 Thermo Scientific TR-5MS capillary column coupled to a Thermo Scientific ISQ QD MS
187 unit. The analysis and quantification of reactants and product concentrations (C_j) were
188 done using a 7890A Agilent Technologies GC equipped with a FID detector and a
189 Supelcowax-10 30M capillary column. Response factors were calculated using solutions
190 containing weighted amounts of the different reactants (FAME, short carbon chain
191 alcohols) and products (FOL) and the standard (n-hexadecane) were injected in the GC.

192 Methyl oleate conversion (X_{MO}^t) was calculated as:

$$193 \quad X_{MO}^t (\%) = \frac{n_{MO}^0 - n_{MO}^t}{n_{MO}^0} \cdot 100 \quad (\text{Eq. 1})$$

194 where n_{MO}^0 are the moles of methyl oleate initially loaded to reactor and n_{MO}^t are the
195 moles of MO at the reaction time t . Selectivities to products j (S_j^t) classically defined as
196 shown in Equation 2:

197
$$S_j^t (\%) = \frac{n_j^t}{n_{MO}^0 - n_{MO}^t} \cdot 100 \quad (\text{Eq. 2})$$

198 were calculated in practice according to Equation 3:

199
$$S_j^t (\%) = \frac{c_j^t}{\sum C_j^t} \cdot 100 \quad (\text{Eq. 3})$$

200 since $\frac{n_{MO}^0 - n_{MO}^t}{\text{Volume}} = \sum C_j^t$. In Equation 3, C_j^t is the concentration of product j at reaction
201 time t .

202 Product yields (Y_j^t) were calculated according to Equation 4:

203
$$Y_j^t (\%) = \frac{X_{MO}^t (\%) S_j^t (\%)}{100} \quad (\text{Eq. 4})$$

204 The initial methyl oleate conversion rate (r_{MO}^0 , mol/hg_{cat}) was calculated from the
205 initial slope of the X_{MO} vs. time curve after multiplication by n_{MO}^0/W , according to:

206

207
$$r_{MO}^0 = \left[\frac{d X_{MO}}{d \left(\frac{tW}{n_{MO}^0} \right)} \right]_{\frac{tW}{n_{MO}^0} = 0} \quad (\text{Eq. 5})$$

208

209 where n_{MO}^0 is the number of moles of methyl oleate in the reactor at $t = 0$ and W the
210 catalyst load.

211

212 **2.5. Computational details for theoretical study of FOL synthesis mechanism**

213 Density functional theory (DFT) molecular orbital calculations were performed using
214 the B3LYP/6-31++G(d,p) level theory [Lee et al.,1988] with Gaussian 09 software
215 package [Frisch et al., 2016]. An initial conformational optimization was performed for
216 the reactants, products and transition state (TS) geometries to obtain the lowest energy
217 conformation.

218 The theoretical study of the reaction mechanism was carried out, optimizing the
219 reactants, products, transition states and intermediate states. Looking for the transition
220 states, the frequencies of the optimized structures were calculated in order to verify that
221 one of them is negative. We confirmed that all the reactants, intermediates, and products
222 have no imaginary frequencies whereas each transition state has only one imaginary
223 frequency. Energies values presented and discussed in this work are Gibbs free energies,
224 because Gibbs free energies include thermal correction to the electronic energies, as well
225 as the entropic factor.

226 For modeling purposes, a shorter saturated methyl ester, methyl acetate, was used as
227 FAME. Each reaction mechanism step that was studied is composed of reactants,
228 transition state, intermediate state and products. We treated the reaction in the gas phase
229 and all thermochemical parameters were calculated at 298 K and 1 atm.

230

231 **3. Results and discussion**

232 ***3.1. Catalyst characterization***

233 Pure Al_2O_3 and $x\text{MAI}$ catalysts were characterized in their chemical, textural,
234 structural and acid-base properties. Results obtained are presented in Table 1. The
235 chemical analysis, carried out by ICP, shows that catalyst metal loadings vary between
236 7.0 and 8.9 wt.%, which are close to the desired nominal content (8.0 wt.%). All catalytic
237 solids exhibit surface areas (SA) lower than that of the alumina support ($230 \text{ m}^2/\text{g}$) and
238 vary between 53 and $173 \text{ m}^2/\text{g}$. This result suggests a pore blockage produced by metallic
239 species added during impregnation preparation method.

240 Structural properties of the solids were analyzed by XRD technique and the results
241 obtained for all samples investigated are shown in Figure 1. The XRD analysis of 7.7FeAl
242 and 7.0CeAl catalysts, showed signals attributable to incipient crystalline phases of Fe_2O_3

243 (JCPDS-ICDD 34-192), AlFeO_4 (JCPDS-ICDD 84-2153) and CeO_2 (JCPDS-ICDD 81-
244 792), respectively, in addition to the amorphous phase of the $\gamma\text{-Al}_2\text{O}_3$ support. On the
245 other hand, diffractogram of 8.9MoAl do not show crystalline phases of Mo incorporated
246 on the $\gamma\text{-Al}_2\text{O}_3$ during impregnation, suggesting that the Mo species are dispersed on the
247 surface of the support even with contents close to 8.9 wt.%.

248 The surface acid and basic properties of the $x\text{MAI}$ samples were investigated by CO_2
249 TPD and NH_3 TPD techniques, respectively. The desorption profiles of both probe
250 molecules are shown in Figure 2. The CO_2 TPD profiles (Figure 2A) show that most
251 solids exhibit a single desorption peak centered at low temperature (360-400 K). This
252 result suggests that their basicity is weak. The number of total basic sites (n_b , $\mu\text{mol/g}$)
253 was determined by integration of the CO_2 desorption profiles and are presented in Table
254 1. As can be seen, the n_b value of the $\gamma\text{-Al}_2\text{O}_3$ support is low (19 $\mu\text{mol/g}$), in agreement
255 with previously reported results [i Díez et al., 2003]. On the other hand, as expected, the
256 promotion of the support with metal cations with recognized Lewis acid properties, in
257 general decreases the basic properties of the solids (Table 1). In effect, in all cases n_b
258 values of $x\text{MAI}$ are lower than that of alumina varying from 1 to 16 $\mu\text{mol/g}$.

259 On the other hand, the NH_3 TPD profiles (Figure 2B) exhibit a broad desorption peak
260 between 500-900 K indicates the presence of acid species that adsorb NH_3 with different
261 binding energies. Al_2O_3 support exhibits two peaks at 480 and 615 K, corresponding to
262 weak and strong acid sites, respectively. Solids 7.7FeAl and 7.0CeAl also exhibit two
263 desorption peaks at 585 and 833 K. These results suggest that $x\text{MAI}$ catalytic solids
264 exhibit strong acidity. The total acid site number (n_a , $\mu\text{mol/g}$) was determined by
265 integration of the NH_3 desorption profiles and are presented in Table 1. All the solids
266 showed n_a values higher than that of the support (24 $\mu\text{mol/g}$).

267 The acid properties of Lewis nature of the solids caused by incorporation of M^{n+}

268 cations, were theoretically evaluated considering the ionic potential q/r (Table 1). This
269 parameter, defined as the quotient between the charge and the radius of each of the cations
270 [Bernal et al., 2008], takes the lowest value for 7.0CeAl sample and the highest for
271 8.9MoAl catalyst. Evidence that this parameter allows visualizing the acidity of the
272 catalysts is its relationship with the n_a values. In fact, in Figure 3 it can be seen that n_a
273 increases monotonically with q/r .

274 In summary, observing in Table 1 the results obtained during the characterization of
275 the acid-base properties and data taken from literature for 8.9MoAl [Inmanee et al., 2017],
276 results evident that within the series of xMAl catalysts investigated, 8.9MoAl exhibits the
277 highest Lewis acidity.

278

279 ***3.2. Non-catalytic reduction of methyl oleate using pure NaBH₄***

280 In a previous work [Vallejo Orrego et al., 2020] we demonstrated that fatty alcohol
281 (FOL) synthesis can be performed through non-catalytic fatty acid methyl ester (FAME)
282 reduction experiments without H₂ supply. Through these experiments it was possible to
283 elucidate the roles of NaBH₄ and methanol in FAME reduction. Both reactants allow
284 forming alkoxyborohydride species which are better reducing agents than NaBH₄. We
285 also postulated a mechanism for methyl laurate reduction and which is shown adapted for
286 any FAME in Scheme 1. The effect of FAME structure was also investigated in this
287 previous work employing methyl laurate (ML), methyl myristate (MM) and methyl oleate
288 (MO). Results obtained showed that the lowest final FAME conversion was achieved
289 using MO which barely reached 34.5%. As expected, the only FOL obtained from ML
290 and MM were lauryl alcohol and myristyl alcohol, respectively; i.e., the saturated FOL,
291 reaching in both cases selectivities of 100%. Surprisingly, using methyl oleate as starting
292 FAME oleyl alcohol was exclusively obtained, i.e., the selectivity towards unsaturated

293 FOL was 100%. This result allowed us to conclude that $\text{NaBH}_4/\text{Al}_2\text{O}_3$ contributes to the
294 selective reduction of C=O bond preserving C=C bond of MO.

295 In this work, the experiments are focused on optimization of the MO reduction reaction
296 using NaBH_4 as reducing agent (hydride donor) and methanol (proton donor). The MO
297 reduction reaction is shown in Scheme 2 where the stoichiometric ratio involved is
298 depicted. Our goal was to improve the low final MO conversion (X_{FAME}) and FOL yield
299 (Y_{FOL}) values obtained using MO as the starting FAME in our previous work [**Error!**
300 **Marcador no definido.** Vallejo Orrego et al., 2020].

301 The effect of reaction temperature on MO conversion and FOL yield was firstly
302 investigated. These experiments were carried out using typical methanol/ NaBH_4 and
303 FAME/ NaBH_4 molar ratios of 6.0 and 0.28, respectively. Figure 4 shows the MO
304 conversion evolution with reaction time obtained at 308, 320 and 333 K. In all
305 experiments, selectivity towards unsaturated FOL (oleyl alcohol) was 100%. Results
306 from Figure 4 and Table 2 show an increase of final methyl oleate conversion (X_{MO}) and
307 final oleyl alcohol yield (Y_{OA}) as reaction temperature increases from 308 to 333 K. In
308 effect, the X_{MO} values reached at end of reaction (6 h) were 31.9, 40.2 and 58.6%,
309 respectively (Table 2). Reaction temperature can not be increased above 333 K working
310 at atmospheric pressure due that the boiling temperature of methanol co-reactant (338 K).

311 From the analysis of reaction temperature effect can be concluded that 333 K is the
312 most appropriate temperature to carried out MO reduction and it was adopted to perform
313 optimization of experimental conditions.

314 After optimizing the reaction temperature, the effect of MO/ NaBH_4 molar ratio was
315 investigated. During these experiments pure NaBH_4 , a molar ratio methanol/ NaBH_4 of
316 6.0, MO/ NaBH_4 molar ratios of 0.11, 0.28 and 0.72 and a reaction temperature of 333 K
317 were used. The evolution of MO conversion with reaction time for each MO/ NaBH_4

318 molar ratio is shown in Figure 5. The oleyl alcohol (S_{OA}) was the only product observed
319 in all experiments. The best results were obtained working with an excess of NaBH_4
320 respect to the stoichiometric ratio 1:1 indicated in the reaction pathway of Scheme 2.
321 Results from Figure 5 also show that the higher the excess of the reducing agent, the
322 higher the final OA yield. In fact, results from Table 2 show that the final FOL yield
323 increases from 21.4% to 93.9% by decreasing the MO/NaBH_4 molar ratio from the 0.72
324 to 0.11.

325 In a previous work, we obtained similar results during reaction condition optimization
326 using methyl laurate (ML) as starting FAME [Vallejo Orrego et al., 2020] and in all
327 experiments. In those experiments, the selectivity toward FOL was 100% and ML
328 conversions at 6 h of reaction were 72, 78, and 98%, respectively.

329 The conversion of methyl oleate to fatty alcohols was previously studied. In most of
330 these works the reaction strategy is the catalytic hydrogenation using high pressures of
331 gaseous H_2 (0.1 and 8 MPa) and high temperatures (473-563 K). Thus, in some of them
332 expensive catalysts involving noble metals such as $\text{Ru-Sn}/\text{Al}_2\text{O}_3$ [Echeverri et al., 2011;
333 Pouilloux et al., 1996; Narasimhan et al., 1989; Mazzieri et al., 2010], $\text{Ru-Ge}/\text{Al}_2\text{O}_3$
334 [Sánchez et al., 2013] have been employed. Final yields toward unsaturated alcohol (oleyl
335 alcohol) were generally low and varied between 12 and 60% being the saturated FAME
336 (methyl stearate) and saturated alcohol (stearyl alcohol) the main products obtained.
337 Other authors used mono and bimetallic catalysts based in no-noble metals supported on
338 different oxides, such as Co/ZnO , Sn/ZnO , $\text{Co}/\text{Al}_2\text{O}_3$, $\text{Co-Sn}/\text{Al}_2\text{O}_3$, $\text{Co-Sn}/\text{ZnO}$, Co-
339 Sn/SiO_2 [Pouilloux et al., 1998; Pouilloux et al., 2000; De Oliveira et al., 2001; De
340 Oliveira et al., 2012]. Using these catalysts, MO hydrogenation yields mainly heavy esters
341 (oleyl oleate) being the yields toward oleyl alcohol low (11-51%).

342 Different authors investigated metal hydrides as effective reducing agents of C=O
343 compounds using short carbon chain alcohols [Soai et al., 1982; Soai et al., 1984; Brown
344 et al., 1982; Rajeswara Rao et al., 1987; Xu et al., 2010], but the raw materials to be
345 reduced in these cases were ethyl caproate and ethyl benzoate [Brown et al., 1982] using
346 different metal hydrides or esters and lactones using NaBH₄ [Soai et al., 1982; Soai et al.,
347 1984]. However, very few works are known in the open literature that have investigated
348 methyl oleate (MO) reduction using metal hydrides as reducing agents. In effect, McKee
349 et al. [McKee et al., 2019] and Xin et al. [Xin et al., 2021] investigated MO reduction
350 using cobalt chloride/sodium borohydride and Ni-La-B systems, respectively, but these
351 studies lead methyl stearate as main product (reduction of C=C bond) and not produce
352 the most value product (unsaturated alcohol). The best result during methyl oleate
353 reduction to the corresponding unsaturated FOL (oleyl alcohol, OA) using NaBH₄ or
354 LiAlH₄ and methanol was obtained by Rajeswara Rao et al. [Rajeswara Rao et al., 1987],
355 reaching a final yield toward oleyl alcohol of 72%. However, in these works authors do
356 not investigate fully the effect that different reaction conditions have on oleyl alcohol
357 selectivity and yield during MO reduction. Here, we achieved promising results during
358 the reduction reaction of methyl oleate to the unsaturated fatty alcohol (oleyl alcohol)
359 making for the first time, a huge effort in analyzing the effect of reaction conditions
360 during optimization of OA synthesis through non-catalytic MO reduction.

361

362 ***3.3. Methyl oleate reduction using NaBH₄ supported on xMAI catalysts.***

363 In previous paragraphs the optimization of reaction conditions during oleyl alcohol
364 (OA) synthesis from methyl oleate (MO) using NaBH₄ and without supplying H₂ gas was
365 described. However, despite the high MO conversion values obtained at the end of the
366 reaction in experiments carried out at 333 K and with a molar ratio MO/NaBH₄ of 0.11,

367 initial FAME conversion values were low, as we could be concluded analyzing the slopes
368 at the origin of the conversion vs. time curves of Figures 4 and 5.

369 Previously, a mechanism for the reduction of FAME in using NaBH_4 and methanol as
370 co-reactants was proposed [Vallejo Orrego et al., 2020]. Briefly, the initial stage of
371 mechanism consists in the formation of the reducing species: alkoxyborohydride anions.
372 The second stage involves the successive steps that allow the interaction between the
373 reducing species and the FAME, leading to the formation of FOL. FAME (MO)
374 conversion to FOL (OA) requires reducing species that allow the reduction of the C=O
375 carbonyl group of FAME. To do this, NaBH_4 interacts with methanol generating
376 alkoxyborohydride species $[\text{BH}_{4-n}(\text{CH}_3\text{O})_n]^-$ ($n = 1, 2, 3$) that are more effective reducing
377 agents than the borohydride anion $[\text{BH}_4]^-$, as concluded from results obtained previously
378 [Vallejo Orrego et al., 2020]. This reducing effect increases each time a methoxy group
379 is attached to $[\text{BH}_4]^-$ species. After reducing species formation, MO is activated via the
380 interaction between C=O group and the dimethoxyborohydride anion. The hydride
381 addition of the reducing species originates a tetrahedral intermediate anion, which
382 immediately interacts with the B atom of an incipient species of $\text{BH}(\text{OCH}_3)_2$ through a
383 polar B-O bond. By subsequent removal of a methoxide specie, which is incorporated
384 into the dimethoxyborohydride anion, an aldehyde intermediate is formed, which rapidly
385 is reduced by interaction with the trimethoxyborohydride anion. Indeed, the H^- of the
386 reducing species attacks the carbon of the C=O group of the aldehyde leading to the
387 formation of a tetrahedral intermediate anion and the tetramethoxyborate species. In the
388 last part of mechanism, another methanol molecule protonates this tetrahedral
389 intermediate to form oleyl alcohol. In order to address the study of the mechanism from
390 a theoretical approach, slight modifications were made to the successive steps described
391 above, which will be described later.

392 Taking into account that postulated mechanism, metal cations have been incorporated
393 to Al_2O_3 before the incorporation of the co-reactant NaBH_4 , and thus, $x\text{MAl}$ catalysts
394 were synthesized. The goal was to increase the acidity and thus favor the polarization of
395 the $\text{C}=\text{O}$ group of the ester and the $[\text{BH}_4]^-$ anion bond facilitating the formation of
396 reducing species and their attack on the $\text{C}=\text{O}$ of the ester. The requirements of these metal
397 cations to favor polarization are: 1) to have a low ionic radius; 2) to possess high charge.
398 With this in mind, the 7.0CeAl, 7.7FeAl and 8.9MoAl catalysts were tested in the
399 reduction of MO to OA. Figure 6 shows the evolution of MO conversion with reaction
400 time on these solids, while Table 2 summarizes the final yields to OA (Y_{OA}) and the initial
401 conversion rates of FAME (r_{MO}^0) obtained. In all cases the selectivity to FOL were 100%.
402 The 8.9MoAl solid exhibits the highest final OA yield value. In fact, this catalyst reached
403 a Y_{OA} of 81.6% after 6 h reaction (Table 2), which is higher than the obtained on Al_2O_3
404 ($Y_{OA} = 53.0\%$).

405 On the other hand, the reduction of MO on 7.0CeAl and 7.7FeAl catalysts allow to
406 obtain lower OA final yield (48.8% and 58.7%, respectively). This result confirms that,
407 in order to favor the bond polarization of the functional groups involved in the reaction,
408 small metallic cations with high charge are required, that is, high q/r values. On the other
409 hand, structural features, characterizes by XRD analysis (Figure 1 and Table 1), would
410 influence in catalytic results since $x\text{MoAl}$ is the only catalyst where metal species are well
411 spread out on the surface of the support.

412 The effect of the surface acid-base properties and cation polarizing power (q/r
413 parameter) of $x\text{MAl}$ solids on the catalytic activity was also investigated. In this way, the
414 initial MO conversion rate was related with n_b , n_a , and q/r . Results obtained are shown in
415 Figure 7A and 7B and Table 2. Results from Table 2 show that 8.9MoAl is the most active
416 catalysts during MO reduction. This was evidenced through its high value of r_{MO}^0 (0.20

417 mol/hg), which favored a rapid formation of reducing species that concludes with
418 obtaining the non-reducing anion $[\text{B}(\text{OCH}_3)_4]^-$ and therefore the Y_{OA} increases more
419 slowly up to reach a final value of 81.6%. A similar behavior is exhibited by the 7.7FeAl
420 catalyst, which showed high activity (Table 2) and therefore, the final Y_{OA} is rapidly
421 reached after 2 h of reaction (Figure 6).

422 The catalytic activity of $x\text{MAI}$ solids (r_{MO}^0) seems not to correlate clearly with n_b
423 values, although apparently a maximum appears for 8.9MoAl catalyst (Figure 7A). In
424 general, this result suggests that surface basic sites would not be directly involved in the
425 conversion of MO to OA. On the other hand, Figure 7B clearly shows that r_{MO}^0 values
426 increase as n_a and q/r increase, suggesting that the M^{n+} cations whose nature have higher
427 polarizing power (q/r values) and that are found in greater quantity on the surface of the
428 catalyst (n_a values) are those that promote the polarization of the ester $\text{C}=\text{O}$ and anion
429 $[\text{BH}_4]^-$ bonds.

430

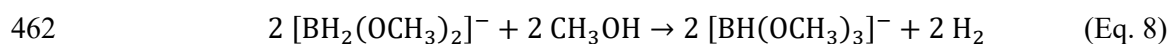
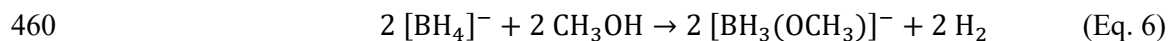
431 ***3.4. Molecular modeling by DFT of reaction steps involved in fatty alcohol synthesis***

432 The reaction mechanism proposed for FAME reduction was studied from a theoretical
433 approach. The molecular modeling was carried out optimizing reactants, products,
434 transition states and intermediate states. During the search for the transition states (TS),
435 the frequencies of the optimized structures were calculated in order to verify that one of
436 them was negative. The result of this frequency was contrasted with the movement of the
437 atoms involved in the reaction in order to confirm that this structure belonged to a
438 transition state.

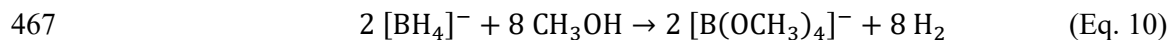
439 As previously mentioned, the calculations were made using methyl acetate as model
440 molecule to represent FAME, whose reduction using NaBH_4 would lead toward ethanol
441 (model molecule for FOL). The purpose of this choice is to decrease the size of the

442 calculations involved reducing both the time needed as well as the computational
 443 resources. During calculations it was possible to establish a general balance of atoms
 444 between reactants and products from the generation of the reducing species toward the
 445 formation of the alcohol through interaction of FAME (methyl acetate) and
 446 alkoxyborohydride species, and thus, was possible to normalize the free Gibbs energies
 447 as a function of the energy of the initial reactants [Foresman et al., 2015] (ΔG , Kcal/mol).

448 In the first instance, the mechanism for reducing species (alkoxyborohydrides)
 449 generation was evaluated, taking into account that in each step, methanol is part of the
 450 reactants and there is hydrogen generation. In effect, the investigated methanolysis
 451 reaction involves, two moles of borohydride anion $[\text{BH}_4]^-$ and eight moles of methanol
 452 (CH_3OH) as starting reactants and two moles of tetramethoxyborate anion $[\text{B}(\text{OCH}_3)_4]^-$
 453 and eight moles of hydrogen (H_2) as reaction products. The initial step of the global
 454 mechanism for FAME reduction (also for methyl acetate) comprises a series of sub-steps
 455 in which the anion $[\text{BH}_4]^-$ reacts with methanol through successive reactions to produce
 456 initially the monosubstituted anion $[\text{BH}_3(\text{OCH}_3)]^-$ and hydrogen (Scheme 3), until the
 457 fully substituted anion $[\text{B}(\text{OCH}_3)_4]^-$ is reached. The successive steps involved in
 458 methanolysis reaction and used to perform the calculations are represented by Equations
 459 6 to 9,



464 while Equation 10 represents the global methanolysis reaction of $[\text{BH}_4]^-$ of sodium
 465 borohydride that has been widely discussed in the literature [Demirci et al., 2010;
 466 Fernandes et al., 2009; Lo et al., 2007]:



468 Since there is no information available about the coordinates of a structure that
469 represents a transition state that allows to simplify the calculations, a special strategy was
470 used to start the calculations. This strategy involves the use of synchronous quadratic
471 transit method (TSQ) [Foresman et al., 2015; Devia, 2018; Barroso, 2021] which consists
472 of finding a possible transition state from the coordinates of reactants, products and
473 optionally a third molecule corresponding to a supposed transition state. The coordinates
474 of the two reactants ($[\text{BH}_4]^-$ and methanol) and the two products ($[\text{BH}_3(\text{OCH}_4)]^-$ and
475 hydrogen) involved were first used, however, it failed to reach a satisfactory transition
476 state at negative energy and frequencies. Consequently, it was decided to build a pseudo-
477 transition state that resembled the reactants and products structures. Then, verifying the
478 presence of a single imaginary frequency and confirming that the energy of the structure
479 results higher than the energy of the reactants and products, this first structure was taken
480 as the basis for calculating the other transition states involved in methanolysis.

481 Figure 8A shows the initial optimized geometries of anionic borohydride species
482 $[\text{BH}_4]^-$, alkoxyborohydrides $[\text{BH}_{4-n}(\text{OCH}_3)_n]^-$ ($n = 1, 2$ and 3), tetramethoxyborate
483 $[\text{B}(\text{OCH}_3)_4]^-$ and the compounds methanol, methyl acetate, acetaldehyde and ethanol. In
484 addition, optimized structures obtained during the sub-steps of reaction pathway
485 presented in Scheme 3, including the corresponding transition state TS1, TS2, TS3 and
486 TS4, in which the bonds that are formed and broken are represented with dotted lines, are
487 presented in Figure 8B.

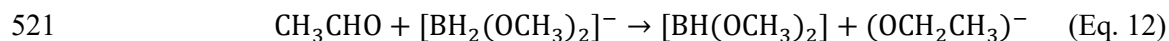
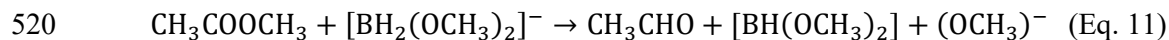
488 On the other hand, Figure 9 shows the progress of all steps involved in methyl acetate
489 reduction mechanism through the various intermediates and its different energy levels on
490 the potential energy diagram (PED), where the energy of the structures is represented as
491 a function of the reaction coordinate. Total Gibbs free energy of eight methanol

492 molecules, two $[\text{BH}_4]^-$ species, one hydrogen atom and one methyl acetate molecule has
493 been considered as the reference of the reaction in the energy profile ($\Delta G = 0$ Kcal/mol).

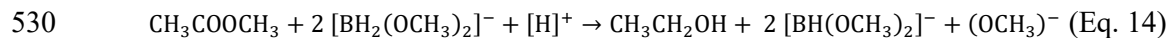
494 As can be seen, the formation of each alkoxyborohydride and tetramethoxyborate
495 species proceed spontaneously, i.e., they are reaction steps that are energetically favored
496 and therefore do not require an energy supply to be carried out. These results are
497 consistent with the experimental results presented in the literature on $[\text{BH}_4]^-$ methanolysis
498 [Ocon et al., 2013; Kaya et al., 2019]. The transition states found during the theoretical
499 study of the generation of reducing species have an imaginary frequency, the movement
500 of their atoms are consistent with formation of products and they have an energy higher
501 than the sum of the energies of the reactants or products. This allows us to conclude that
502 these structures correspond to the transition states (TS) of the reaction. In general, in the
503 transition states, the H^- from the borohydride or methoxyborohydride anion and the H^+
504 from methanol react to form gaseous hydrogen and the following substituted
505 alkoxyborohydride species. In conclusion, the results obtained in the generation of the
506 reducing species from theoretical calculations are in total agreement with the mechanism
507 proposed from experimental evidence in Scheme 1.

508 After studying, from a theoretical point of view, the formation of the reducing species,
509 we evaluated the second part of the mechanism proposed in Scheme 1, which consists of
510 obtaining the fatty alcohol from the reduction of the ester. Considering that methyl acetate
511 is used as a model ester to represent FAME, the aldehyde that would be formed in the
512 first stage of the mechanism would be acetaldehyde and the alcohol that would be
513 generated as the final product would be ethanol. In order to simplify the analysis of the
514 interaction of reducing species with FAME (Scheme 1), to facilitate understanding of the
515 theoretical approach in the reaction pathway of Scheme 3 and taking into consideration
516 the time required to perform and analyze the results of the calculations, the theoretical

517 analysis that was carried out involves the species $[\text{BH}_2(\text{OCH}_3)_2]^-$ as unique reducing agent
518 of methyl acetate and acetaldehyde. Taking the above into account, Equations 11, 12 and
519 13 detail the sub-steps involved in the formation of ethanol.



523 Equation 11 represents the general expression to obtain the first intermediate of the
524 reaction, which corresponds to acetaldehyde for the model proposed in this study. As
525 shown in the Scheme 3, acetaldehyde in turn is rapidly reduced by $[\text{BH}_2(\text{OCH}_3)_2]^-$ species
526 or by another alkoxyborohydride species to form an ethoxide intermediate $(\text{OCH}_2\text{CH}_3)^-$
527 (Scheme 3), which is then converted to ethanol by H^+ from methanol. This last part of the
528 process is represented in Equations 12 and 13. General equation representing the whole
529 process is depicted in Equation 14:



531 In order to evaluate their energetic behavior and compare theoretical results of
532 calculations with the proposed experimental mechanism, frequencies of all the molecules
533 involved in each sub-step of the mechanism were calculated. For the TS5, TS6, TS7 and
534 TS8, the existence of an imaginary frequency (negative value) in the structures proposed
535 as a TS was verified.

536 Analysis of the results obtained in the theoretical calculation carried out on the
537 synthesis of ethanol was divided for a better understanding into two steps: formation of
538 the acetaldehyde intermediate and formation of the final product, ethanol.

539 To form acetaldehyde from methyl acetate, the presence of a nucleophilic compound
540 containing H^- ions is necessary to transfer electrons to the carbonyl group of the ester.
541 Results obtained are shown in Figures 8 and 9. The transition state TS5 is initially formed

542 from the attack of the anion $[\text{BH}_2(\text{OCH}_3)_2]^-$ to the C=O bond of methyl acetate (Figure
543 8B); then an intermediate (EI1 in Figure 8C) is formed in which the H^- forms a single
544 bond to the C=O group at the same time that the other single bond C-O between carbon
545 and the leaving group $(\text{OCH}_3)^-$ of methyl acetate begins to break, leaving the oxygen of
546 the C=O with negative charge. In the second transition state (TS6) formation, the C=O
547 bond is reformed and the $(\text{OCH}_3)^-$ group is lost (Scheme 3) leading to acetaldehyde
548 $[\text{BH}(\text{OCH}_3)_2]$ and $(\text{OCH}_3)^-$ species.

549 Figure 9 shows that the acetaldehyde formation results an exergonic reaction and is
550 energetically favored, since the products have a lower energy state ($\Delta G = -100.1$
551 Kcal/mol) than the reactants ($\Delta G = -53.9$ Kcal/mol).

552 The last part of ethanol formation mechanism requires the initial formation of an
553 ethoxide intermediate through reduction of acetaldehyde and then, the last step, involves
554 its conversion into ethanol (Scheme 3). The ethoxide formation (Equation 12) is
555 represented in Figure 8B while Figure 9 shows the energy profile as a function of the
556 reaction coordinate. As can be seen in Figure 8B, for the conversion of acetaldehyde (P5)
557 to ethoxide intermediate (EI2), a transition state (TS7) is formed in which a H^- of the
558 species $[\text{BH}_2(\text{OCH}_3)_2]^-$ attacks the carbon of acetaldehyde C=O group.

559 This approximation favors the breaking of alkoxyborohydride B-H bond and the
560 formation of the C-H bond that gives rise to ethoxide species. Ethoxide is considered an
561 intermediate between acetaldehyde and ethanol, in which the carbon atom of the C=O
562 group forms three bonds: two simple C-H bonds and other bond that corresponds to the
563 partial formation of a double bond between carbon and oxygen, in which the oxygen atom
564 meets delocalized electrons that would favor the formation of ethanol. Results presented
565 in Figure 9 show that the energy change involved in going from P5 to EI2 is not
566 energetically favored to form the ethoxide, indicating that this step requires extra energy

567 to be carried out. The fact that this structure is not energetically favored confirms that it
568 is a reaction intermediate state. The final sub-step of the reaction involves the formation
569 of ethanol (Equation 13). Calculation results obtained on this step are shown in Figures
570 8B and 9. To carry out the theoretical calculations in this sub-step, the H atom of methanol
571 was used as a proton source, which, as was verified in the theoretical studies of
572 methanolysis steps comes from the alcohol O-H group. On the other hand, in the
573 mechanism showed in Scheme 3, the H⁺ of methanol participates in both the generation
574 of hydrogen and the alcohol formation. Thus, structures of Figure 8B show that in the
575 transition state (TS8), the H atom approaches the ethoxide to favor the formation of the
576 O-H bond leading to ethanol. Furthermore, in Figure 9 allow concluding that alcohol
577 formation occurs exergonically and thus, this sub-step is energetically favored.

578 In conclusion, the mechanism involved in the generation of reducing species was
579 theoretically elucidated. In this part of global mechanism, it was possible to confirm the
580 formation of alkoxyborohydride species is energetically favored. Furthermore, the results
581 obtained during the theoretical calculations for ethanol formation through methyl acetate
582 reduction, allowed us to understand the events at the microscopic level involved in the
583 mechanism of the reaction under study. In addition, the exhaustive study of the sub-steps
584 involved in the mechanism confirmed the formation of several structures
585 (alkoxyborohydride, acetaldehyde and ethoxide species) which act as intermediate
586 compounds in obtaining alcohol. Finally, reducing the size of the system in the theoretical
587 study allows to reach a first approach to the intermolecular interactions that exist between
588 the different species involved in the reduction of shorter ester than FAME; during
589 extrapolation of this theoretical study involving the synthesis of ethanol toward the
590 synthesis of fatty alcohols (FOL) derived from FAME, it was possible to confirm the

591 analysis carried out at macroscopic level (experimental results) by proposing in Scheme
592 1 the reaction mechanism for FOL synthesis.

593

594 **4. Conclusions**

595 Oleyl alcohol (OA) synthesis could be improved through non-catalytic and catalytic
596 experiments with selectivities of 100% from methyl oleate and methanol using both
597 unsupported NaBH₄ and catalyst-supported NaBH₄. In order to optimize the synthesis,
598 different reaction conditions (temperature, methyl oleate/NaBH₄ molar ratio and catalyst
599 nature) were employed without the supply of H₂ gaseous. Thus, in non-catalytic
600 experiments a final yield of the valuable unsaturated fatty alcohol OA of 93.9% was
601 achieved using a methyl oleate/NaBH₄ molar ratio of 0.11 and a reaction temperature of
602 333 K.

603 The effect of the incorporation of different metal cations M (M = Fe, Ce, Mo) to the
604 alumina support on the activity and OA yield was studied and it was found that
605 8.9Mo/Al₂O₃ solid, the catalyst with the highest acid site number and the highest
606 polarizing power, allow obtaining the best activity value. In fact, this catalytic solid favors
607 the C=O bond polarization of the ester and the anion [BH₄]⁻ to form the actual reducing
608 species that then interact with the methyl oleate.

609 Reaction mechanism previously postulated for fatty acid methyl esters reduction
610 towards fatty alcohols using methanol and NaBH₄ was studied in this work from a
611 theoretical approach using density functional theory (DFT) method at B3LYP/6-
612 31++G(d,p) computational level. Calculations were made using methyl acetate as model
613 molecule to represent fatty acid methyl esters, whose reduction would lead toward ethanol
614 (model molecule for fatty alcohols). This choice allowed to decrease the size of the
615 calculations involved, reducing both the time needed as well as the computational

616 resources. It was possible to confirm that the formation of reducing alkoxyborohydride
617 species is energetically favored. On the other hand, results obtained during the theoretical
618 calculations for ethanol formation from methyl acetate, allowed to understand the events
619 at the microscopic level involved in the reaction mechanism studied. Finally, it was
620 possible demonstrate, that the reduction of the system size during the theoretical study
621 allows to reach a first approach to the intermolecular interactions that exist between the
622 different species involved in the acetate reduction. During extrapolation of the DFT study
623 performed for ethanol synthesis toward the fatty alcohol synthesis from fatty acid methyl
624 esters, we confirmed the analysis carried out at macroscopic level based on experimental
625 results.

626

627 **Acknowledgements**

628 Authors thank the Agencia Nacional de Promoción Científica y Tecnológica
629 (ANPCyT), Argentina (Grant PICT 2015-1857), Consejo Nacional de Investigaciones
630 Científicas y Técnicas (CONICET), Argentina and Universidad Nacional del Litoral
631 (UNL), Argentina (Grant CAI+D 2016 50420150100029LI) for financial support of this
632 work.

633

634 **Authorship**

635 **V.K.D.** Conceived and designed the study; conceptualized, supervised and analyzed the
636 data; and wrote the first draft of the manuscript. **C.A.F.** Conceptualized and supervised
637 theoretical research (DFT) and analyzed the data. **A.V.O.** Carried out the experimental
638 and theoretical research and analyzed the data. All authors contributed to and approved
639 the final draft of the manuscript.

640

641 **Declaration of Competing Interest**

642 The authors declare that they have no known competing financial interests or personal
643 relationships that could have appeared to influence the work reported in this paper.

644

645 **References**

646 Barroso Joaquin's Blog. Available from: <https://joaquinbarroso.com/> [accessed 3rd
647 February 2021].

648 Bernal J.P., Railsback L.B., Introducción a la Tabla Periódica de los Elementos y sus
649 Iones para Ciencias de la Tierra, Rev. Mex. Ciencias Geológicas. 2008; 25:236-246.

650 Brown H.C., Narasimhan S., Choi Y.M., Selective Reductions. 30. Effect of Cation and
651 Solvent on the Reactivity of Saline Borohydrides for Reduction of Carboxylic Esters.
652 Improved Procedures for the Conversion of Esters to Alcohols by Metal Borohydrides,
653 J. Org. Chem. 1982; 47:4702-4708. <https://doi.org/10.1021/jo00145a018>.

654 Demirci U.B., Akdim O., Andrieux J., Hannauer J., Chamoun R., Miele P., Sodium
655 Borohydride Hydrolysis as Hydrogen Generator: Issues, State of the Art and
656 Applicability Upstream from a Fuel Cell, Fuel Cells. 2010; 10:335-350.
657 <https://doi.org/10.1002/fuce.200800171>.

658 De Oliveira K., Pouilloux Y., Barrault J., Selective Hydrogenation of Methyl Oleate into
659 Unsaturated Alcohols in the Presence of Cobalt–Tin Supported over Zinc Oxide
660 Catalysts, J. Catal. 2001; 204:230-237. <https://doi.org/10.1006/jcat.2001.3378>.

661 De Oliveira Vigier K., Pouilloux Y., Barrault J., High efficiency CoSn/ZnO catalysts for
662 the hydrogenation of methyl oleate, Catal. Today. 2012; 195:71-75.
663 <https://doi.org/10.1016/j.cattod.2012.04.027>.

664 Devia I.C.R., Determinación del estado de transición en la reacción de oxidación del n-
665 heptano con el catalizador [MnAcO(C₁₆H₁₄N₂O₂)] mediante la exploración de la

666 superficie de energía potencial, Universidad de Ciencias Aplicadas y Ambientales,
667 2018.

668 Díez V.K., Apesteuguía C.R., Di Cosimo J.I., Effect of the chemical composition on the
669 catalytic performance of Mg_yAlO_x catalysts for alcohol elimination reactions, *J. Catal.*
670 2003; 215:220-233. [https://doi.org/10.1016/S0021-9517\(03\)00010-1](https://doi.org/10.1016/S0021-9517(03)00010-1).

671 Echeverri D.A., Rios L.A., Marín J.M., Síntesis de alcoholes grasos insaturados a partir
672 de metilésteres grasos usando catalizadores a base de rutenio y estaño soportados sobre
673 alúmina, *Ing. e Investig.* 2011; 31:74-82.

674 Fernandes V.R., Pinto A.M.F.R., Rangel C.M., Hydrogen production from sodium
675 borohydride in methanol-water mixtures, *Int. J. Hydrogen Energy.* 2009; 35:9862-
676 9868. <https://doi.org/10.1016/j.ijhydene.2009.11.064>.

677 Foresman J.B., Frisch A., *Exploring Chemistry With Electronic Structure Methods*, 3rd
678 ed., Gaussian Inc., Wallingford, CT; 2015.

679 Frisch M.J., Trucks G.W., Schlegel H.B., Scuseria G.E., Robb M.A., Cheeseman J.R.,
680 Scalmani G., Barone V., Petersson G.A., Nakatsuji H., Li X., Caricato M., Marenich
681 A., Bloino J., Janesko B.G., Gomperts R., Mennucci B., Hratchian H.P., Ortiz J.V.,
682 Izmaylov A.F., Sonnenberg J.L., Williams-Young D., Ding F., Lipparini F., Egidi F.,
683 Goings J., Peng B., Petrone A., Henderson T., Ranasinghe D., Zakrzewski V.G., Gao
684 J., Rega N., Zheng G., Liang W., Hada M., Ehara M., Toyota K., Fukuda R., Hasegawa
685 J., Ishida M., Nakajima T., Honda Y., Kitao O., Nakai H., Vreven T., Throssell K.,
686 Montgomery J.A. Jr., Peralta J.E., Ogliaro F., Bearpark M., Heyd J.J., Brothers E.,
687 Kudin K.N., Staroverov V.N., Keith T., Kobayashi R., Normand J., Raghavachari K.,
688 Rendell A., Burant J.C., Iyengar S.S., Tomasi J., Cossi M., Millam J.M., Klene M.,
689 Adamo C., Cammi R., Ochterski J.W., Martin R.L., Morokuma K., Farkas O.,

690 Foresman J.B., Fox D.J., Gaussian 09 (Revision A.02), 2016.
691 <https://gaussian.com/glossary/g09/>.

692 Inmanee T., Pinthong P., Jongsomjit B., Effect of Calcination Temperatures and Mo
693 Modification on Nanocrystalline (γ - χ)-Al₂O₃ Catalysts for Catalytic Ethanol
694 Dehydration, J. Nanomater. 2017; Article ID 5018384:9 pages.
695 <https://doi.org/10.1155/2017/5018384>.

696 Kaya M., Bekirogullari M., Investigation of Hydrogen Production from Sodium
697 Borohydride Methanolysis in the Presence of Al₂O₃/Spirulina Platensis Supported Co
698 Catalyst, Eur. J. Sci. Technol. 2019; 16:69-76. <https://doi.org/10.31590/ejosat.549911>.

699 Lee C., Yang W., Parr R.G., Development of the Colle-Salvetti correlation-energy
700 formula into a functional of the electron density, Phys. Rev. B. 1988; 37:785-789.
701 <https://doi.org/https://doi.org/10.1103/PhysRevB.37.785>.

702 Lo C.F., Karan K., Davis B.R., Kinetic Studies of Reaction between Sodium Borohydride
703 and Methanol, Water, and Their Mixtures, Ind. Eng. Chem. Res. 2007; 46:5478-5484.
704 <https://doi.org/10.1021/ie0608861>.

705 Mazzieri V.A., Sad M.R., Vera C.R., Pieck C.L., Preparation and characterization of Ru-
706 Sn/Al₂O₃ catalysts for the hydrogenation of fatty acid methyl esters, Quim. Nova.
707 2010; 33:269-272. <https://doi.org/10.1590/S0100-40422010000200007>.

708 McKee J.R., Zanger M., Chiariello C., McKee J.A., Dorfner W., Fasella E., Koo Y.,
709 Semimicro/Microscale Adaptation of the Cobalt Chloride/Sodium Borohydride
710 Reduction of Methyl Oleate, J. Chem. Educ. 2019; 96:772-775.
711 <https://doi.org/10.1021/acs.jchemed.8b00222>.

712 Miya B. Method of producing copper-iron-aluminum catalysts. US4252689 (Patent),
713 1981.

714 Narasimhan C.S., Deshpande V.M., Ramnarayan K., Selective Hydrogenation of Methyl
715 Oleate to Oleyl Alcohol on Mixed Ruthenium-Tin Boride Catalysts, *Appl. Catal.* 1989;
716 48:L1-L6. [https://doi.org/10.1016/S0166-9834\(00\)80260-2](https://doi.org/10.1016/S0166-9834(00)80260-2).

717 Noweck K., Production, Technologies and Applications of Fatty Alcohols, *Work. Fats*
718 *Oils as Renew. Feed. Chem. Ind.* 2011:1-9.

719 Ocon J.D., Tuan T.N., Yi Y., De Leon R.L., Lee J.K., Lee J., Ultrafast and stable
720 hydrogen generation from sodium borohydride in methanol and water over Fe-B
721 nanoparticles, *J. Power Sources.* 2013; 243:444-450.
722 <https://doi.org/10.1016/j.jpowsour.2013.06.019>.

723 Pouilloux Y., Piccirilli A., Barrault J., Selective hydrogenation into oleyl alcohol of
724 methyl oleate in the presence of Ru-Sn/Al₂O₃ catalysts, *J. Mol. Catal. A Chem.* 1996;
725 108:161-166. [https://doi.org/10.1016/1381-1169\(96\)00010-6](https://doi.org/10.1016/1381-1169(96)00010-6).

726 Pouilloux Y., Autin F., Piccirilli A., Guimon C., Barrault J., Preparation of oleyl alcohol
727 from the hydrogenation of methyl oleate in the presence of cobalt-tin catalysts, *Appl.*
728 *Catal. A Gen.* 1998; 169:65-75. [https://doi.org/10.1016/S0926-860X\(97\)00344-X](https://doi.org/10.1016/S0926-860X(97)00344-X).

729 Pouilloux Y., Autin F., Barrault J., Selective hydrogenation of methyl oleate into
730 unsaturated alcohols relationships between catalytic properties and composition of
731 cobalt-tin catalyst, *Catal. Today.* 2000; 63:87-100.
732 [https://doi.org/https://doi.org/10.1016/S0920-5861\(00\)00448-X](https://doi.org/https://doi.org/10.1016/S0920-5861(00)00448-X).

733 Rajeswara Rao Y., Pantulu A.J., Lakshminarayana G., Reduction of Fatty Acid Methyl
734 Esters with Sodium Borohydride-t-Butanol-Methanol, *Fat Sci. Technol.* 1987; 89:398-
735 400. <https://doi.org/https://doi.org/10.1002/lipi.19870891006>

736 Rieke R.D., Thakur D.S., Roberts B.D., White G.T., Fatty Methyl Ester Hydrogenation
737 to Fatty Alcohol Part I: Correlation Between Catalyst Properties and

738 Activity/Selectivity, J. Am. Oil Chem. Soc. 1997; 74:333-339.
739 <https://doi.org/10.1007/s11746-997-0088-y>.

740 Rieke R.D., Thakur D.S., Roberts B.D., White G.T., Fatty Methyl Ester Hydrogenation
741 to Fatty Alcohol Part II: Process Issues, J. Am. Oil Chem. Soc. 1997; 74:341-345.
742 <https://doi.org/10.1007/s11746-997-0089-x>.

743 Sad M.R., Mazzieri V.A., Vera C.R., Pieck C.L., Hidrogenación selectiva de metil ésteres
744 de ácidos grasos para obtención de alcoholes grasos. I. Perspectivas actuales,
745 catalizadores y mecanismos de reacción, Av. En Química, 2007:17-24.

746 Sánchez M.A., Mazzieri V.A., Oportus M., Reyes P., Pieck C.L., Influence of Ge content
747 on the activity of Ru-Ge-B/Al₂O₃ catalysts for selective hydrogenation of methyl
748 oleate to oleyl alcohol, Catal. Today. 2013; 213:81-86.
749 <https://doi.org/10.1016/j.cattod.2013.02.028>.

750 Soai K., Oyamada H., Ookawa A., Sodium Borohydride-t-butyl Alcohol-Methanol as an
751 Efficient System for the Selective Reduction of Esters, Synth. Commun. 1982; 12:463-
752 467. <https://doi.org/10.1080/00397911.2011.574329>.

753 Soai K., Oyamada H., Takase M., Ookawa A., Practical Procedure for the Chemoselective
754 Reduction of Esters by Sodium Borohydride. Effect of the Slow Addition of Methanol,
755 Bull. Chem. Soc. Jpn. 1984; 57:1948-1953.
756 <https://doi.org/https://doi.org/10.1246/bcsj.57.1948>.

757 Tahara K., Tsuji H., Kimura H., Okazaki T., Itoi Y., Nishiyama S., Tsuruya S., Masai M.,
758 Liquid-phase hydrogenation of dicarboxylates catalyzed by supported Ru-Sn catalysts,
759 Catal. Today. 1996; 28:267-272. [https://doi.org/https://doi.org/10.1016/0920-
760 5861\(95\)00247-2](https://doi.org/https://doi.org/10.1016/0920-5861(95)00247-2).

761 Toba M., Tanaka S., Niwa S., Mizukami F., F. Koppány F., Guzzi L., Cheah K.Y., Tang
762 T.S., Synthesis of alcohols and diols by hydrogenation of carboxylic acids and esters

763 over Ru–Sn–Al₂O₃ catalysts, *Appl. Catal. A Gen.* 1999; 189:243-250.
764 [https://doi.org/10.1016/S0926-860X\(99\)00281-1](https://doi.org/10.1016/S0926-860X(99)00281-1).

765 Vallejo Orrego A., Ferretti C.A., Díez V.K., Reduction of Vegetable Oil-Derived Fatty
766 Acid Methyl Esters toward Fatty Alcohols without the Supply of Gaseous H₂, *JAOCS*,
767 *J. Am. Oil Chem. Soc.* 2020; 97:1029-1042. <https://doi.org/10.1002/aocs.12375>.

768 Xin Z., Wei G., Zhang L., Gao L., Li Z., Zhao W., Partial hydrogenation of fatty acid
769 methyl esters under mild conditions using sodium borohydride as hydrogen donor,
770 *Fuel*. 2021; 299: Article ID 120877. <https://doi.org/10.1016/j.fuel.2021.120877>.

771 Xu Y., Wei Y., CeCl₃-Catalyzed Reduction of Methyl Esters of Carboxylic Acids to
772 Corresponding Alcohols with Sodium Borohydride, *Synth. Commun.* 2010; 40:3423-
773 3429. <https://doi.org/10.1080/00397910903457233>.

774 Yoshino K., Kajiwara Y., Takaishi N., Inamoto Y., Tsuji J., Hydrogenation of Carboxylic
775 Acids by Rhenium-Osmium Bimetallic Catalyst, *J. Am. Oil Chem. Soc.* 1990; 67:21-
776 24. <https://doi.org/10.1007/bf02631383>.

777

778

779

780

781

782

783

784

785

786

787

788 **Captions to Figures and Schemes**

789

790 **Scheme 1.** Reaction mechanism for fatty acid methyl ester reduction using methanol as
791 proton donor and sodium borohydride as hydride donor.

792

793 **Scheme 2.** Stoichiometry of oleyl alcohol (OA) synthesis reaction from methyl oleate,
794 methanol and sodium borohydride.

795

796 **Scheme 3.** Possible mechanisms involved in the methyl acetate reduction reaction used
797 for DFT calculations.

798

799 **Figure 1.** Diffractograms obtained on x MAI samples.

800

801 **Figure 2.** CO₂ TPD (A) and NH₃ TPD (B) profiles for x MAI solids.

802

803 **Figure 3.** Relation between n_a and q/r for x MAI catalysts.

804

805 **Figure 4.** Effect of reaction temperature during methyl oleate conversion to oleyl
806 alcohol (T = 308 K, 320 K, 333 K; FAME/NaBH₄ molar ratio = 0.28; methanol/NaBH₄
807 molar ratio = 6.0; NaBH₄ as reducing solid).

808

809 **Figure 5.** Effect of varying FAME/NaBH₄ molar ratio during methyl oleate conversion
810 to oleyl alcohol (T = 333 K; methanol/NaBH₄ molar ratio = 6.0; NaBH₄ as reducing
811 solid).

812

813 **Figure 6. Figure 6.** MO conversion as a function of reaction time on xMAI catalysts (T
814 = 333 K; MO/NaBH₄ molar ratio = 0.11; methanol/NaBH₄ molar ratio = 6.0; NaBH₄/MAI
815 as reducing solid).

816

817 **Figure 7.** Relation between r_{MO}^0 and n_b (A) and, r_{MO}^0 and q/r and n_a (B) for xMAI
818 catalysts (T = 333 K; MO/NaBH₄ molar ratio = 0.11; methanol/NaBH₄ molar ratio =
819 6.0).

820

821 **Figure 8.** Different optimized initial geometries (A), transitions states (A) and
822 intermediates (C) found for methyl acetate reduction reaction obtained from DFT
823 calculations.

824

825 **Figure 9.** Reaction energy profile for methyl acetate reduction toward ethanol formation
826 obtained from DFT calculations.

827

828

829

830

831

832

833

834

835

836

Table 1. Chemical, textural, structural and acid-base characterization of xMAI catalysts.

| Catalyst | Metal content, x^a (wt. %) | Textural properties | | | Acid-base properties | | | Structural phases detected by XRD |
|----------------------------------|------------------------------|----------------------------|--|---------------------|----------------------|------------------|------------------------|--|
| | | SA^b (m ² /g) | Pore volume, Vg (cm ³ /g) | Pore size, dp (⊕) | n_b^c (μmol/g) | n_a^d (μmol/g) | Ionic potential, q/r | |
| CeAl | 7.0 | 173 | 0.41 | 95.2 | 16 | 111 | 3.96 | CeO ₂ , γ-Al ₂ O ₃ |
| FeAl | 7.7 | 53 | 0.10 | 76.7 | 9 | 128 | 4.62 | Fe ₂ O ₃ , AlFeO ₃ , γ-Al ₂ O ₃ |
| MoAl | 8.9 | 128 | 0.27 | 84.1 | 12 | 977 ^e | 9.68 | γ-Al ₂ O ₃ |
| γ-Al ₂ O ₃ | - | 230 | - | - | 19 | 24 | - | γ-Al ₂ O ₃ |

^a by ICP; ^b BET surface areas; ^c by TPD of CO₂; ^d by TPD of NH₃; ^e from reference [19]

Table 2. Non-catalytic and catalytic results obtained during methyl oleate reduction using NaBH₄.

| Catalyst | Reaction conditions | | | Results obtained during MO reduction | | |
|----------------------------------|--------------------------|-----------------------------------|---|---|---|---|
| | Reaction temperature (K) | MO/NaB H ₄ molar ratio | Methanol/NaB H ₄ molar ratio | <i>S</i> _{OA} ^a (%) | <i>X</i> _{MO} or <i>Y</i> _{OA} ^b (%) | <i>r</i> ⁰ _{MO} ^c (mol/hg) |
| - | 308 | 0.28 | 6.0 | 100.0 | 31.9 | - |
| - | 320 | 0.28 | 6.0 | 100.0 | 40.2 | - |
| - | 333 | 0.28 | 6.0 | 100.0 | 58.6 | - |
| - | 333 | 0.11 | 6.0 | 100.0 | 93.9 | - |
| - | 333 | 0.72 | 6.0 | 100.0 | 21.4 | - |
| γ-Al ₂ O ₃ | 333 | 0.11 | 6.0 | 100.0 | 53.0 | 0.16 |
| CeAl | 333 | 0.11 | 6.0 | 100.0 | 48.8 | 0.16 |
| FeAl | 333 | 0.11 | 6.0 | 100.0 | 58.7 | 0.18 |
| MoAl | 333 | 0.11 | 6.0 | 100.0 | 81.6 | 0.20 |

^a during the whole 6-hour experiment; ^b at t = 6 h; ^c Initial MO conversion rate (at t = 0).